Magnetic correlations of fine ferromagnetic particles studied by small-angle neutron scattering

C. Bellouard
Laboratoire de Métallurgie Physique et Science des Matériaux (URA CNRS 155), Université de Nancy 1, BP 239, 54506 Vandoeuvre-lès-Nancy Cédex, France

I. Mirebeau and M. Hennion
Laboratoire Léon Brillouin (CEA-CNRS), CE Saclay, 91191 Gif-sur-Yvette Cédex, France
(Received 20 June 1995; revised manuscript received 18 September 1995)

We have performed small-angle x-ray and neutron scattering of fine Fe particles embedded in an alumina matrix. For the sample with the lowest Fe content (volumic fraction 20%), x-ray scattering reveals a well-defined peak, characterizing a liquidlike short-range order between particles of similar size, with a chemical radius of 10 Å. The magnetic radius of the particles and their magnetization, as measured by neutron scattering, increases with decreasing temperature, due to the alignment of spins at the surface. Below 100 K, ferromagnetic correlations start to develop between near-neighbor particles. For higher particle densities (volumic fraction 35% and 47%), the nanoparticles coexist with larger aggregates, yielding two typical particle sizes in the same sample. Here, the interparticle correlations persist up to the highest measured temperature (500 K). Such correlations could arise from the dipolar field, which increases with decreasing temperature, as observed by inelastic neutron scattering.

I. INTRODUCTION

The interest in artificially grown samples is continuously increasing due to the expectation of new magnetic properties. Concerning magnetic nanocrystalline materials, there has been intense activity these last years both in applied and fundamental physics since the discovery of giant magnetoresistance or macroscopic quantum tunneling. Besides such phenomena, there is a fundamental interest in the study of systems where single-domain particles may be considered as huge magnetic spins. This is illustrated, for instance, by the well-known superparamagnetic properties, first described by Néel,[1] for granular ferrites. Due to the existence of an energy barrier related to the anisotropy, the particle magnetization fluctuates as a whole from one easy magnetization axis to another.[2,3] More generally, the possibility of varying the particle size or the distance between particles allows one to play with interparticle interaction effects, or conflicting effects between single-particle anisotropy and interparticle interactions. Small-angle neutron-scattering technique has been previously used to measure the shape anisotropy of precipitates[4] or to observe the particle correlations induced by an applied field in some ferrofluids.[5,6] It provides a direct observation of the correlations between particles in zero magnetic field. These come either from dipolar forces if the particles are imbedded in an insulating matrix, or by indirect exchange ones if this matrix is metallic. Moreover, inelastic neutron scattering, which usually requires large sample quantities to obtain measurable intensities, can take full advantage from the particle form factor. Since the magnetic intensity is gathered in a small-q range of reciprocal space, it may become possible, when the time scale of fluctuations is adequate, to observe the global dynamics of these particles. Several techniques can be used to prepare fine particles like cosputtering or coevaporation, chemical processes or lithography. Independently of the technique, however, a severe limitation in this experimental field comes from the difficulty of preparing monodispersed particles.

Here we report a small-angle scattering study by x-rays and neutrons of Fe particles of nanometer size dispersed in an alumina matrix. For one sample with an Fe volume fraction of 20%, which can be considered as quasimonodispersed, we perform a quantitative analysis. This reveals two distinct phenomena: one related to the temperature dependence of the single-particle magnetization, and the other to interparticle correlations which grow at low temperature. Our results are an improvement over previous studies which have been performed in a smaller q range.[7,8] We also report a qualitative study of two more concentrated alloys (30% and 35%) with larger particles. In these two latter samples, the Fe concentration is close to the percolation point and the particles coexist with larger aggregates as shown by x-ray diffraction. In spite of this inhomogeneity, the results in these two samples confirm the trends observed in the quasimonodispersed one.

We divide the paper as follows. In Sec. II, we describe the characterization of the samples, and give experimental details. In Sec. III, we report our experimental observations for the sample with 20% of Fe, and propose a quantitative analysis. In Sec. IV, we study the influence of the Fe concentration. In Sec. V, we discuss overall results in comparison with the results from inelastic neutron scattering, whose full description will be presented in a following paper.

II. EXPERIMENTAL DETAILS

A. Sample description and characterization

We have studied three samples, denoted $S1$, $S2$, and $S3$ in the following, corresponding to 20%, 35%, and 47% volumic fractions of iron, respectively. They consist of iron particles embedded in an amorphous alumina matrix, deposited on an alumina substrate. They have been prepared by

TABLE I. Sample characterization by magnetization. The iron weight percentage is determined with the Castaing probe; the oxidized Fe (10%) located in the alumina or at the sample surface has been excluded. The volume fraction ρ_v is evaluated from the Fe wt % and from the density of bcc iron and amorphous alumina. r_m is the radius deduced from magnetization measurements. d_m is the distance between particle centers estimated from the r_m and ρ_v values, assuming a compact arrangement between the particles. T_B is the temperature of the peak in the low-field ($H \leqslant 50$ Oe) susceptibility measured after a zero-field cooling.

Samples	$S1$	$S2$	$S3$
Fe wt %	48%	65%	75%
ρ_v	20%	35%	47%
r_m (Å)	12.5±1	25±2	37±3
d_m (Å)	38	65	86
T_B (K)	15±1	136±1	⩾300

cosputtering.[9] The substrate and sample thicknesses are 30 and 18 μm, respectively. The samples have been characterized by magnetic measurements. The blocking temperatures T_B, corresponding to the maximum low-field susceptibility, measured after cooling the sample in zero field, are 15, 136, and above 300 K, respectively, as reported in Table I. From the field dependence of the magnetization, we have determined the average particle radius, using the high- and low-field approximations of the Langevin function.[10] As shown in Table I, the measured mean volume of the particles increases with increasing Fe content in agreement with the increase of T_B. Actually, the relaxation time of the particle, roughly given at $T=T_B$ by the characteristic time of the measurement, is a function of the ratio KV/kT_B, where K is the anisotropy constant. The proportionality between V and T_B thus indicates that the anisotropy constant, arising from single-particle anisotropy or interaction effects, is roughly the same for the three samples.

B. Small-angle x-ray scattering (SAXS)

The SAXS measurements were performed in the Laboratoire de Physique de la Matière Condensée, at the College de France, with an incident wavelength of 1.54 Å corresponding to the Cu $K\alpha$ line, and a linear multidetector of 93 cells. The range of the scattering vector q was 0.03–0.6 Å^{-1}. The spectra were deconvoluted from the response function of one cell. The raw intensity I_{raw} was corrected from the scattering of the substrate I_{sub}, using the following formula:

$$I_{\text{corr}} = I_{\text{raw}} - \frac{T_{\text{sample}}}{T_{\text{sub}}} I_{\text{sub}}, \tag{1a}$$

where T corresponds to the transmission. The incident flux Φ_0 has been measured with an absorbent sample. Then we calculated the differential cross section $d\sigma/d\Omega$ in absolute units, using the formula

$$I_{\text{corr}} = t T_{\text{sample}} \Phi_0 d\Omega \frac{d\sigma}{d\Omega}, \tag{1b}$$

where t and $d\Omega$ are the sample thickness and the solid angle corresponding to one cell, respectively.

C. Small-angle neutron scattering (SANS)

SANS measurements were performed on the spectrometer *PAXY* of the laboratoire Léon Brillouin at the reactor Orphée, with an *XY* multidetector of 128×128 cells, and an incident wavelength of 5 Å. The corresponding incident energy (3 meV) is much higher than the typical energies of the inelastic magnetic processes, as measured by inelastic neutron scattering (0.01 and 0.5 meV). Therefore, the scattering process integrates over all the energy states of the system, yielding the instantaneous spin correlations. Moreover, the small energy transfers related to the magnetic excitations allow us to assume that the q value determined from the position of the detector cell is the real q value.

By varying the sample-detector distance (1.3 and 6.8 m), we have investigated two overlapping q ranges, namely [0.0074, 0.06 Å^{-1}] and [0.04, 0.3 Å^{-1}]. The corresponding sets of data are called high-angle and low-angle measurements in the following. Since the scattering of all samples is isotropic in q space, the intensities corresponding to cells equidistant from the incident beam were gathered, in order to decrease the statistical error. The temperature was varied between 500 and 10 K using an oven and a cryogenerator with the same background conditions.

For sample $S1$, the raw data of the low- and high-angle measurements were corrected for the scattering of the substrate according to Eq. (1a), with $T_{\text{sample}}=T_{\text{sub}}=0.9$. The scattering of an uncoated substrate was measured for the two q ranges. For the high-angle spectrum, this intensity is very small with respect to that of the sample. For the low-angle spectrum, the signal of the substrate alone increases strongly at very low angles. This is due to inhomogeneities, dislocations, or textures, whose contribution could be much larger than the Fe/Al_2O_3 signal and is not reproducible from one substrate to another. Therefore, we have determined the substrate contribution at low angles by using the sample measurements at 500 K. Here the Fe/Al_2O_3 signal is small and q independent below 0.06 Å^{-1}, and thus can be easily evaluated and subtracted, using the high-angle data in the overlapping q range. After the correction of the data at all temperatures from the substrate scattering, we have scaled the low-angle spectra to the high-angle ones, with a scaling factor which never exceeds 1.1, in order to obtain a unique set of data. The neutron intensity was converted in absolute units by measuring the incoherent scattering of a standard nickel sample.

For samples $S2$ and $S3$, where the iron concentration is higher, the signal of the particles is much larger than the substrate contribution, whatever the q range concerned. After correction for the scattering of the uncoated substrate, the low-angle spectrum was scaled to the high-angle one at 300 K. We have kept the same scaling factor for the other temperatures.

III. RESULTS FOR THE SAMPLE WITH 20% FE

A. X-ray measurements

The q dependence of the intensity measured for sample $S1$ is plotted in Fig. 1. If there were no correlations between the positions of the particles, this intensity should decrease monotonically with q, according to the form factor of one

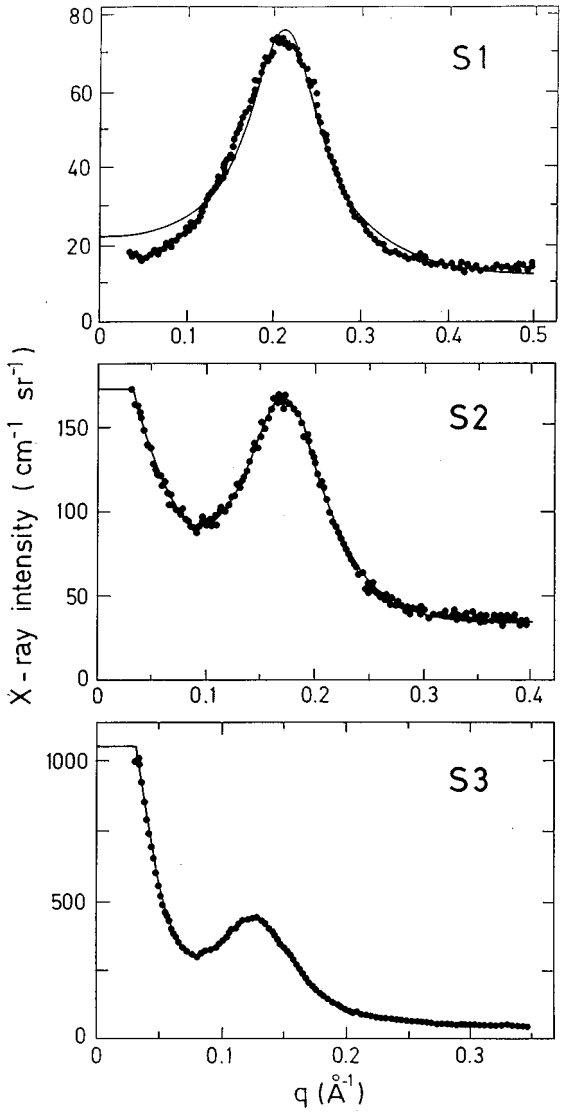

FIG. 1. X-ray intensity of samples $S1$, $S2$, and $S3$. The straight lines correspond to the fits.

particle. As shown in Fig. 1, we observe a well-defined maximum at a q value of about 0.2 Å^{-1}, which corresponds to a short-range order between particles of similar size, closely packed in a liquidlike state. Accordingly, assuming an assembly of identical spherical particles, we have fitted the cross sections by the formula[11]

$$\frac{d\sigma}{d\Omega}=(r_e)^2N\Delta\rho^2V^2F^2(q,r_n)I(q,N,d_{\min})+C, \qquad (2)$$

where r_e is the classical radius of the electron, N the density of particles, $\Delta\rho$ the difference of electronic densities between the particle and the matrix, V is the volume of one particle, $F(q,r_n)$ its chemical form factor, and r_n its chemical radius. $I(q,N,d_{\min})$ is the Aschkroft and Lekner interference function.[12] It corresponds to a liquidlike arrangement of the particles, and depends on N and on the minimal distance of approach or "excluded diameter" $d_{\min}$. C is a flat background term.

In sample $S1$, we note that the fitted curve does not reproduce the experimental data perfectly, especially at small angles, where the experimental points clearly lie below the fit. This is attributed to the roughness of the model used, mainly to some inadequation of the Aschkroft and Lekner interference function. The parameters deduced from the fit are listed in Table II. We can check that the particle radius (r_n=9.5 Å), the minimum distance of approach ($d_{\min}$=29 Å), and the mean distance between the particles (d_n=38 Å), verify the inequality $2r_n<d_{\min}<d_n$. We have determined d_n from the concentration N of the particles, through the relation $d_n^3=\sqrt{2}/N$, valid for a closed-packed structure. This value is in excellent agreement with the value from magnetization data, d_m=38 Å, as reported in Table I, which was found in a similar way by using the relation $d_m^3=4\sqrt{2}r_m^3/3\rho_v$, where ρ_v=20% is the volumic fraction. However, we notice that the x-ray determination of the radius (r_n=9.5 Å) is slightly smaller than its estimation from magnetic measurements (r_m=12.5 Å). The underestimation of the radius made by x rays is mostly attributed to inhomogeneities at the surface of the particles, perhaps to an amorphous layer of Fe and alumina. This would yield a slightly inhomogeneous iron density [instead of the constant one assumed in Eq. (2)], and also a narrow distribution in the particle sizes. In this case, one must realize that, because of the interference function, x rays are mostly sensitive to the large-q tail of the form factor, and thus to the smaller sizes, whereas magnetic measurements probe the $q=0$ contribution.

TABLE II. Parameters deduced from the analysis of the x-ray spectra. $\Delta\rho$ (electron number per Å^3) is the contrast of electronic density between the particles and the matrix. $d_{\min}$ is the exclusion diameter. N is the density of particles. d_n is the mean distance between particles assuming a compact arrangement ($d_n^3=\sqrt{2}/N$). r_n is the radius deduced from the fit of the interference peak.

Samples	$S1$	$S2$	$S3$
Fe wt %	48%	65%	75%
$\Delta\rho$	1.96	1.9	2.5
$d_{\min}$ (Å)	29	34	44
N (Å^{-3})	2.5×10^{-5}	1.4×10^{-5}	0.51×10^{-5}
d_n (Å)	38		
r_n (Å)	9.5	12	15

Thanks to a calibration of the cross section in absolute units, from the mean electronic contrast we can deduce a relation between the iron and alumina densities d_{Fe} and $d_{\mathrm{Al_2O_3}}$.

$$\Delta\rho=10^{-24}\left(\frac{n_{\mathrm{Fe}}d_{\mathrm{Fe}}}{M_{\mathrm{Fe}}}-\frac{n_{\mathrm{Al_2O_3}}d_{\mathrm{Al_2O_3}}}{M_{\mathrm{Al_2O_3}}}\right), \qquad (3a)$$

where M_{Fe} and $M_{\mathrm{Al_2O_3}}$ and n_{Fe} and $n_{\mathrm{Al_2O_3}}$ are the atomic masses and atomic numbers of iron and alumina, respectively.

Another relation is deduced from the measurement of the average density d_{av} ($d_{\mathrm{av}}=3.6\pm0.6$ g/cm^3), namely

$$d_{\mathrm{av}}=\left(\frac{\rho_v}{d_{\mathrm{Fe}}}+\frac{1-\rho_v}{d_{\mathrm{Al_2O_3}}}\right)^{-1}. \qquad (3b)$$

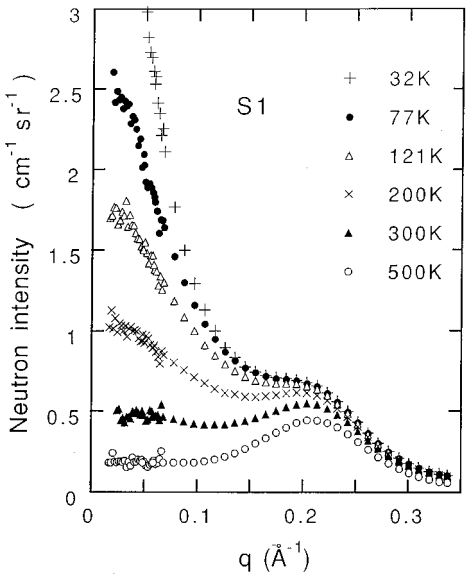

FIG. 2. Neutron intensity $I(q)$ of sample $S1$ after correction of the substrate scattering for several temperatures.

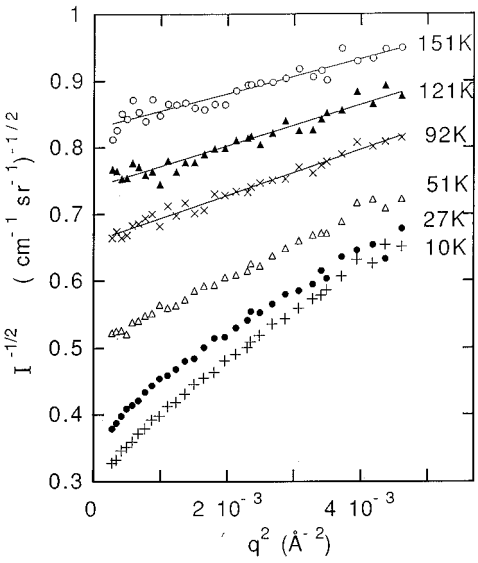

FIG. 3. $1/\sqrt{I}$ as a function of q^2 for $q<0.07$ Å^{-1}, where I is the intensity scattered by sample $S1$.

A graphic resolution of these two equations yields the densities $d_{\mathrm{Fe}}=9.6\pm2$ g/cm^3 and $d_{\mathrm{Al_2O_3}}=2.3\pm0.6$ g/cm^3. The large error bars are due to the uncertainty about the absolute value of the neutron cross section (15%) and the sample volume (10%). Within these error bars, d_{Fe} is comparable to the value of bcc iron (7.8 g/cm^3). $d_{\mathrm{Al_2O_3}}$ is much smaller than the value for crystalline alumina (3.98 g/cm^3), as expected for an amorphous sputtered material. This shows that the model used is rather suitable, and especially that the assumption of a spherical form factor is reasonable, at least in the large-q range.

B. Neutron measurements

1. Results

First of all, we qualitatively describe the spectra. This description clearly shows the temperature variations of the magnetization at a microscopic scale, and justifies the more quantitative analysis described below.

The q dependence of the corrected spectra is plotted in Fig. 2. At low-q values, the intensity strongly depends on temperature, and decreases monotonically with increasing q. At higher-q values, we observe a temperature-independent peak similar to the one studied by x rays. This peak is clearly of nuclear origin. In contrast, the low-q intensity is of course magnetic. The range of its q dependence is the expected one for the squared form factor of one particle. This suggests that the magnetic moments of neighboring particles are *uncorrelated*. In this case, the increase of the low-q intensity with decreasing temperature would correspond to an increase of the density of magnetization of the particles or to an increase of their effective magnetic volume. The first effect would be due to spin waves, the second to the growth of spin correlations at the particle surface.

As shown in Fig. 1, the nuclear signal is negligible in the low-q range ($q<0.07$ Å^{-1}). Therefore, we have characterized the q and T dependences of the magnetic intensity by considering the low-q values only, and have plotted $1/\sqrt{I}$ versus q^2 for $q<0.07$ Å^{-1} (Fig 3). Above 100 K, $1/\sqrt{I}$ varies linearly with q^2, showing that the magnetic signal follows a squared Lorentzian law. Below 100 K, $I(q)$ increases much more strongly, and we observe deviations from this law at very small angles. This suggests the onset of an additional signal, with a higher correlation length, which we attribute to correlations between the moments of neighboring particles.

2. Analysis

First, we analyze the intensity at 300 K, where the global moments of the particles seem to be uncorrelated, implying that they can be considered paramagnetic atoms. For unpolarized neutrons, the total intensity is the sum of the nuclear and magnetic contributions, and we have described its q dependence by the formula

$$I(q)=AI(q,N,d_{\min})F^2(q,r_n)+\left(\frac{r_0}{g\mu_B}\right)^2\tfrac{2}{3}NM_p^2F_m^2(q,r_m). \tag{4}$$

The first term, which corresponds to the nuclear signal, is similar to the one used in the analysis of the x-ray data. It involves the spherical form factor $F(q,r_n)$ and the interference function I described above. In the second term, $r_0=\gamma e^2/mc^2=0.5410^{-12}$ cm. The expression of the magnetic contribution is analogous to the one used for paramagnetic spins.[13] Instead of the usual form factor of the atomic spin, we have inserted in (4) the magnetic form factor of the particle $F_m(q,r_m)$ (the iron form factor is very close to one in our q range). The atomic spin S (Ref. 13) is replaced by the particle spin S_p, which is related to the saturated magnetization density m_s, and to the global particle moment M_p through the expression

$$S_p(S_{p+1})=M_p^2/(g\mu_B)^2, \tag{5}$$

where $M_p=m_sV_p$, and V_p is the volume of the particle. Whatever the shape assumed in the following for the particle

magnetic form factor, the nuclear parameters (r_n, $d_{\min}$) are found to have the same values as in the x-ray experiment, which justifies the above decomposition.

In a first step, we have assumed a unique, spherical, magnetic form factor, as in Ref. 8. At 300 K, this analysis yields a magnetic radius r_m of 9 Å close to the nuclear one (r_n=9.5 Å), and a reasonable value for the magnetic moment (2.2 $\pm$0.4 μB/Fe). However, below 300 K the magnetic intensity starts to increase very steeply, and it becomes clear that the shape assumed for the magnetic form factor is not suitable, especially at low angles. We have then tried to introduce a log-normal distribution of (spherical) magnetic form factors, to account for a possible size distribution. In this case, the moment of the particle has been fixed to the value obtained from magnetization measurements. This procedure improves the quality of the fit, but the average magnetic radius *decreases* with temperature, which is unphysical.

In a second step, for F_m we have taken a Lorentzian-like shape, $[F_m(q)=\kappa_1^2/(q^2+\kappa_1^2)]$, considered here as an analytical approach of the magnetic form factor in our experimental q range. The parameter κ_1^2 at the numerator is introduced for normalization (F_m=1 for q=0). This shape is mostly justified by the qualitative analysis reported above, which shows that it yields a good fit to the data in the small-q range. Of course, this function cannot be identified as the Fourier transform of uniform magnetic density in a finite volume. However, the squared Lorentzian $F_m^2(q)$, which represents the intraparticle correlations, is proportional to the Fourier transform of an exponential law $\langle \hat{S}_0 \hat{S}_r \rangle \propto \exp(-\kappa_1 r)$. Therefore, the magnetic correlation length $\xi_1=1/\kappa_1$, which describes the spin correlations *inside* the particle, should have a close relation with its radius. With this analysis, we obtain good fits to the data down to 100 K.

We note that, in a purely superparamagnetic system with uncorrelated particles, or in a purely ferromagnetic one with perfectly aligned particles moments, we expect a homothetic increase of the magnetic intensity with decreasing T, proportional to the squared particle moment $M^2(T)$. Below 100 K, deviations from the Lorentzian law suggest that we must take into account the onset of magnetic correlations *between the particles*. To describe such correlations, we can make, as before, an analogy with the paramagnetic case, the physical picture being similar but at a different scale. The q dependence of the magnetic signal is expressed as the product of the squared particle form factor with the Fourier transform of the interparticle correlations. We have kept the same form factor as above 100 K, and have described the interparticle correlations by a simple Lorentzian. For a correlated paramagnet, this Lorentzian function corresponds to the Fourier transform of the spin correlations function $\langle \hat{S}_0 \hat{S}_r \rangle \propto [\exp(-\kappa_2 r)]/r$, where the correlation length $\xi_2=1/\kappa_2$ is much larger than the atomic size. Here the use of this function is purely phenomenological. Actually, this term alone is unsufficient, and we must keep a single-particle contribution even below 100 K. This is an important difference from the behavior of typical paramagnets. Its origin can be explained by the specific properties of the fluctuating particles, as discussed below.

Within these assumptions, we can analyze the intensity in the whole q and temperature range with the *same* expression:

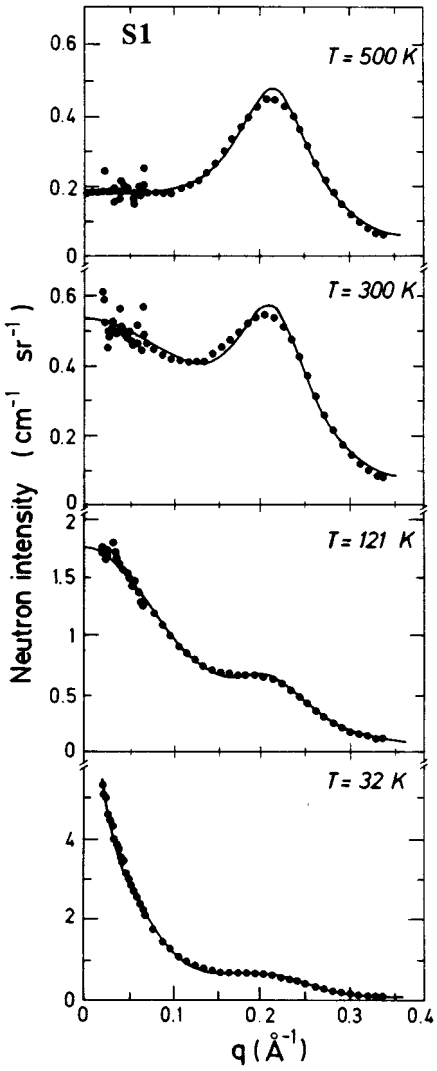

FIG. 4. Neutron intensity of sample $S1$ for several temperatures (500, 300, 121, and 32 K). The straight lines are fits to the data using Eq. (6).

$$I(q)=AI(q,N,d_{\min})F^2(q,r_n)+\frac{\kappa_1^4}{(q^2+\kappa_1^2)^2}\left[B+\frac{C}{q^2+\kappa_2^2}\right]. \tag{6}$$

The A term contains the nuclear signal (and a possible magnetic contribution from perfectly aligned near-neighbor particle moments, not explicitly taken into account here). The B term corresponds to the single-particle or incoherent magnetic contribution. The C term involves the coherent contribution from correlated particle moments. When there are no correlations between the particles, C is equal to zero, and B is proportional to the square of the particle moment. When $C\neq 0$, B represents the fraction of the particles or of their magnetic moments, which remain uncorrelated.

In Fig. 4, we show a selection of the data, fitted with Eq. (6) for several temperatures. In the fit of the data at 51 K shown in Fig. 5, we have also plotted the three contributions separately. Good fits are obtained in the whole T range, and yield very reasonable temperature dependences for all the fitted parameters (Figs. 6 and 7). We describe them now, above and below 100 K.

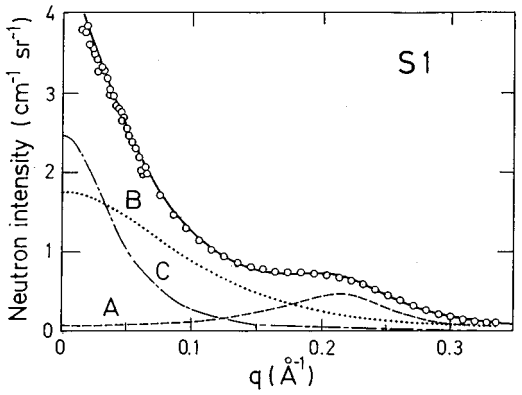

FIG. 5. Neutron intensity of sample $S1$ at 51 K. The straight line is a fit of the data using Eq. (6). The separate contributions to the intensity are also shown: interference term A by the dashed line, Lorentzian term B by the dotted line, and Ornstein-Zernicke term C in the dashed-dotted line.

Above 100 K, the intensity A is constant, as expected for a purely nuclear signal. This ensures that the magnetic form factor is well taken into account by the Lorentzian shape. We have drawn the same conclusion by applying a magnetic field.[14] The intensity B of the magnetic signal steeply increases with decreasing temperature. In Fig. 6, we have compared $\sqrt{B}$, which in the model is proportional to the total magnetic moment of the particle M_p, with its macroscopic determination from high-field measurements. Both quantities show the same variation with temperature. We notice that, with decreasing T, they increase much more steeply than expected for a Brillouin function. From the temperature evolution of $\sqrt{B}$, we determine an increase of the particle moment between 300 and 100 K by a factor of 2. Concomitantly, the correlation length ξ_1 increases with decreasing T, and reaches 6.6 Å at 100 K. We attribute this strong increase of the magnetic moment, and of the magnetic effective volume of the particles, to a progressive alignment of the spins at the surface. This can be related to observations made by inelastic measurements as discussed below.

Below 100 K, we observe a transfer of the magnetic intensity from the uncoherent term (B), to the coherent ones, A and C (see Figs. 6 and 7). The B term related to uncorrelated moments, shows a maximum around 100 K, then decreases. The C parameter, associated with long-range correlations, increases from zero, and we notice an additional magnetic contribution to the interference term A. Clearly, the magnetic moments of neighboring particles start to align, which is also shown by an increase of the interparticle correlation length ξ_2. However, the ξ_2 value remains close to the distance between near-neighbor particles, in contrast to the case of a correlated paramagnet, where ξ_2 is much larger than the atomic scale. From the fit we also obtained a slight decrease of the correlation length ξ_1, associated with the intraparticle correlations, which is unphysical. Therefore, we have kept ξ_1 constant below 100 K, which does not significantly change the quality of the fit.

Besides the exact meaning of the fitted correlation lengths, which remains to be clarified, from this analysis we obtain a self-consistent description of the system, in agreement with magnetic measurements. Moreover, the analysis below 100 K reveals the onset of a magnetic contribution at the nuclear interference peak, when the interparticle correlations develop. This effect, which in sample $S1$ cannot be detected without fitting, is readily shown on the spectra of the two other samples, as discussed now.

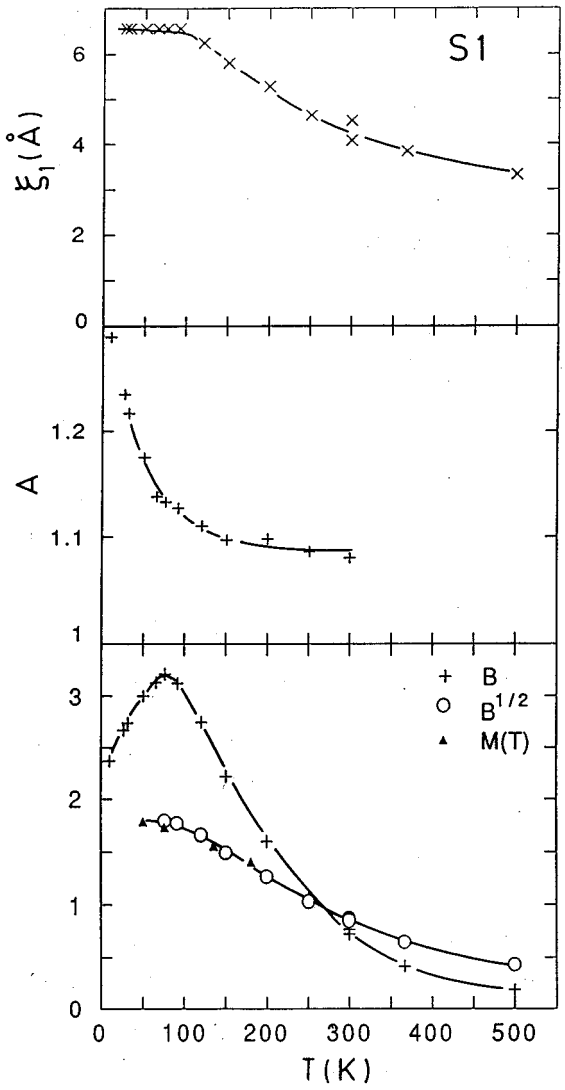

FIG. 6. Temperature dependence of the A, B, $\sqrt{B}$, and ξ_1 parameters deduced from the fit of the $S1$ spectra using Eq. (6). M is proportional to the magnetization of the particle (as determined by magnetization measurements); it has been scaled with $\sqrt{B}$ at $T=136$ K.

IV. INFLUENCE OF THE IRON CONCENTRATION

We now report the results for the two samples with higher Fe contents.

A. X-ray measurements

The spectra for the more dense samples $S2$ and $S3$ are plotted in Fig. 1. We observe, in addition to the interference peak, an increase of the intensity at very small angles. This suggests the coexistence of nanoparticles with much larger entities, which could correspond to particle aggregates. We

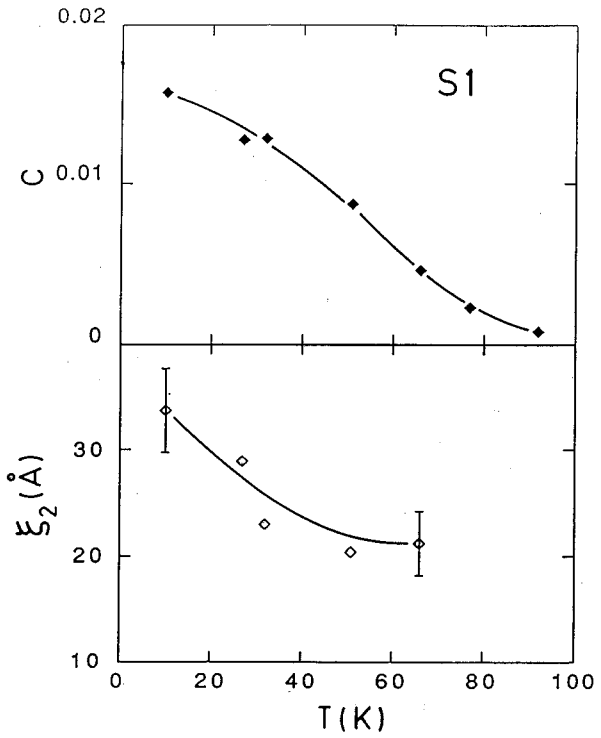

FIG. 7. Temperature dependence of the C and ξ_2 parameters deduced from the fit of the $S1$ spectra using Eq. (6).

have fitted the increase of the intensity at low angles by a Guinier law[11] $\exp[-(R_g q)^2/3]$, where R_g should in principle correspond to the gyration radius of the biggest entities. However, the parameter R_g deduced from the fit does not verify the expected condition $R_g q \ll 1$, and thus has not been reported in Table II. The nanoparticles, which give rise to the interference peak, have a radius r_n of 12 and 15 Å in samples $S2$ and $S3$, respectively. The radii estimated from magnetization data (25 Å) rather correspond to the largest entities.

B. Neutron measurements

Since these two samples do not have monodispersed particles, we could not perform a quantitative analysis of the magnetic signal, as in the first case, and we did not try to fit the data. However, due to the increase in iron concentration, the magnetic contribution is now very large, and we may obtain an insight into its temperature dependence just by looking at the experimental data, without any fit. The qualitative description of the neutron intensities in these two samples gives a strong support to the analysis made for the more dilute one. We observe the same qualitative behavior in the two concentrated samples, as shown in Figs. 8–11.

Since the intensity at small angles is extremely high, we have chosen to display the low- and high-angle data in separate figures, with different intensity scales. Due to this strong magnetic contribution, the shape of the neutron curves is very different from that of the x-ray one. We note that the interference peak is much less pronounced, and that the intensity either increases or decreases with temperature, depending on the q range concerned.

In the very low-q range ($q<0.05$ Å^{-1}), the intensity strongly *increases* with decreasing temperature, from 500 to

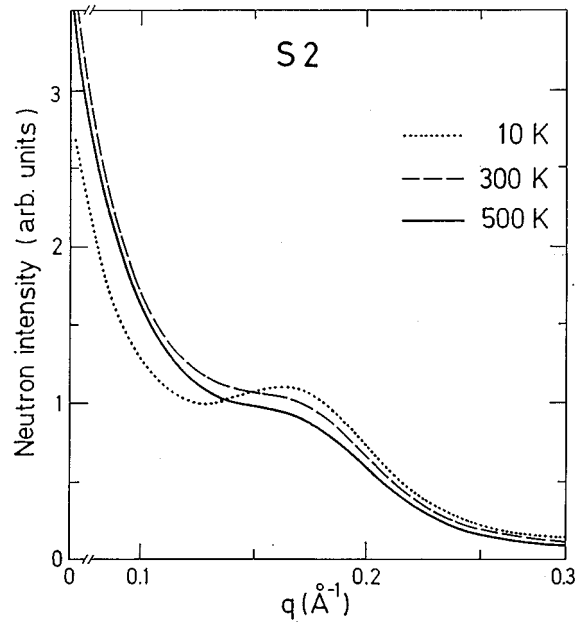

FIG. 8. Neutron intensity in the high-angle q range of sample $S2$ after correction of the substrate scattering for several temperatures.

10 K. In the intermediate-q range ($0.05<q<0.15$ Å^{-1}), we first observe an increase of $I(q)$, between 500 and 300 K, then a *decrease*, when T decreases below 300 K. Finally, in the high-q range ($q>0.15$ Å^{-1}), the intensity increases con-

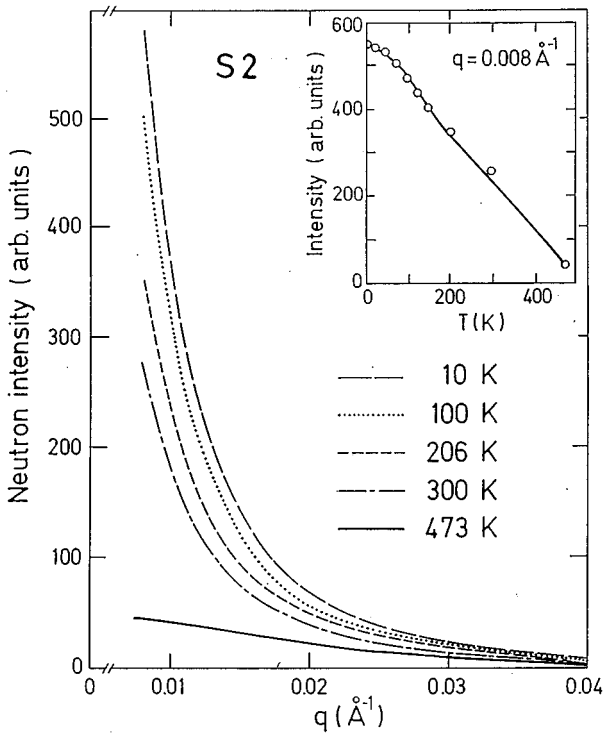

FIG. 9. Neutron intensity in the small-angle q range of sample $S2$ after correction of the substrate scattering for several temperatures. Inset: the intensity for $q=0.008$ Å^{-1} as a function of temperature.

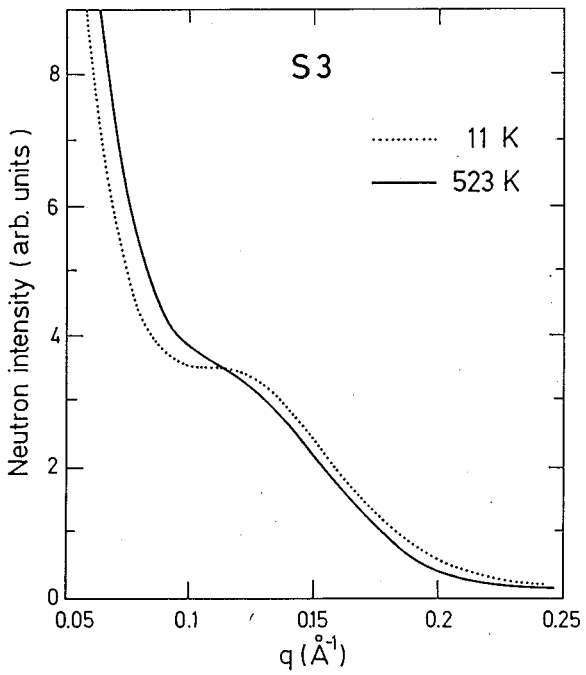

FIG. 10. Neutron intensity in the high-angle q range of sample $S3$ after correction of the substrate scattering for several temperatures.

tinuously with decreasing T, as in the low-q range. Therefore, the curves at 500 and 10 K cross each other in *two* points (around 0.05 and 0.13 Å^{-1}), so that the interference peak is better observed at low temperature. As discussed above, the coherent terms (A and C) are dominant at low-q values and at the peak position, whereas the incoherent one (B) dominates in the mean-q range. When T decreases, the increase of the intensity at low angles and at the peak position is mostly explained by the growing of interparticle correlations. They are expected to be much stronger here than in sample $S1$, due to the higher iron concentration, and thus persist up to 500 K. In the mean-q range, the increase of $I(q)$ between 500 and 300 K is mostly due to an increase of the particle magnetization, which also contributes to the incoherent term. But below 300 K, this effect is shielded by the growing of interparticle interactions, and we observe a decrease of the uncoherent term at the benefit of the coherent ones. Finally, below 100 K, the intensity due to interparticle interactions seems to saturate (see the insets in Figs. 9 and 11). This could be related to a frustration of these interactions, as discussed below in comparison with inelastic measurements.

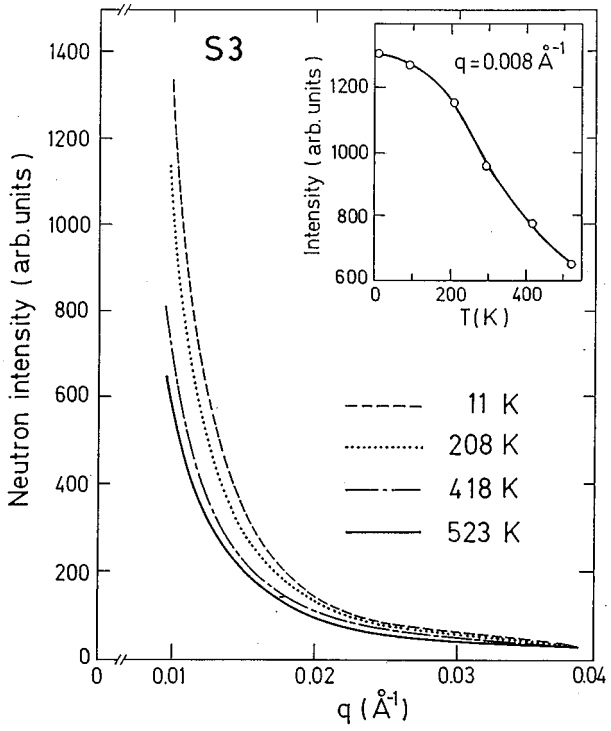

FIG. 11. Neutron intensity in the small-angle q range of sample $S3$ after correction of the substrate scattering for several temperatures. Inset: the intensity for $q=0.008$ Å^{-1} as a function of temperature.

V. DISCUSSION

In summary, we show that the complex evolution of the magnetic correlations of an assembly of very fine particles can be described simply in terms of intraparticle and interparticle correlations. These two effects were already expected from anomalies in the macroscopic measurements. However, thanks to a quantitative analysis which provides the temperature dependence of two magnetic length scales ξ_1 and ξ_2 defined in the system, the neutron observations bring a more precise description and reveal additional features in the temperature evolution. The use of the x-ray technique, complementary to the neutron one, provides a strong support to the quantitative analysis thanks to an independent determination of the nuclear parameters. Our results are in good agreement with those obtained by another group on a similar sample.[7] The sample studied in Ref. 7 was prepared by the same cosputtering technique and its characteristics ($\rho_v=35$ vol% of iron, $r=15$ Å, and $T_B=75$ K) lie in between those of $S1$ and $S2$. It keeps quasimonodispersed particles, and the analytical shape assumed for the neutron intensity is rather close to ours. The authors analyze the magnetic intensity as the sum of two terms $A_1/(q^2+\kappa^2)^2+A_2/q^2$. The $B\kappa_1^4$ term of our analysis, equivalent to A_1, shows the same temperature dependence below 250 K: it decreases with decreasing temperature. However, in our model this decrease is due to a strong increase of the correlation length $\xi_1=\kappa_1^{-1}$, whereas the magnetization $\sqrt{B}$ actually increases with decreasing temperature. The remarkable agreement of $\sqrt{B(T)}$ with the macroscopic magnetization justifies the present analysis *a posteriori*. Of course, the limit of such an analysis comes from the use of a phenomenological lorentzian for the single-particle contribution, instead of a true form factor. This difficulty likely reveals a nonuniform magnetization, in relation to the roughness of the particle surface. The obvious consequence is that ξ_1 cannot be identified as a particle radius. Concerning the interparticle interactions (ξ_2), we show their ferromagnetic character. Actually, this is expected for dipolar forces, as found from a theoretical work[15] which predicts a ferromagnetic order for fcc structures.

We want to stress now that these two distinct phenomena of intraparticle and interparticle effects observed in the q

space can be associated with two distinct dynamical evolutions previously observed in energy space. These have been separated in sample $S1$ using two energy windows.

(i) With an energy resolution of 150 meV, the energy analysis[16] reveals the existence of fast fluctuating spins which gradually freeze below 300 K, as they become more spatially correlated. At high temperature ($T>300$ K), the energy linewidth is nearly temperature independent, and characteristic of quasiparamagnetic spins ($\gamma=0.2$ meV) loosely coupled with soft exchange forces. The effective energy ($J_{\text{eff}}\simeq 25$ K) is much smaller than the expected one for spin waves [T_c(Fe)$=1040$ K]. This reveals the existence of frustrated spins (due to local oxidation or cut bonds at the particle surface). We conclude that the increase of the magnetization and of the particle radius reported above is associated with the freezing of frustrated spins which progressively align with the ferromagnetic core.

(ii) With an energy resolution of 13 meV, the energy analysis[17] reveals two other dynamical components. One, called ''longitudinal,'' is attributed to the magnetization component which relaxes between the metastable states. Its energy becomes resolution limited below 300 K. The other one, called the ''transverse'' component, is attributed to the magnetization component which fluctuates inside the metastable states (it corresponds to a precession at very low temperature). Its energy linewidth, which may be related to the internal field ($\Gamma\simeq g\mu_B H$), provides a temperature-independent value at high temperature (0.01 meV), characteristic of the single-particle anisotropy. It sharply increases below 100 K. This reveals the onset of additional forces in the particle system, attributed to interparticles forces,[18] in excellent agreement with the change in the correlations observed here.

(iii) Since $I(q)$ corresponds to the energy integration of the longitudinal and transverse dynamical components defined above, one easily explains the origin of the single-particle contribution (B term) which persists in the present analysis below 100 K. The huge sensitivity of the relaxation time with the particle volume may significantly prevent in-phase relaxations between some particles even for the quasi-monodispersed sample $S1$. In addition, the transverse magnetization of neighboring particles have been found to fluctuate independently, as shown by the q independency of the energy linewidth. This is found even at low temperature, where the interparticle forces develop.

(iv) In the more concentrated samples, we observe mainly the same behavior as in the $S1$ one. The main difference concerns the interparticle correlations which persist up to the highest measured temperature. At low temperature, we observe a saturation of the intensity related to these correlations. This indicates some competition between interparticle interactions, also suggested by the inelastic neutron study performed on sample $S2$.[19]

ACKNOWLEDGMENTS

We are deeply indebted to J. L. Dormann and C. Djega-Mariadassou for providing the samples and for many fruitful discussions. We also thank A. Brûlet and R. Ober for their help during the neutron and x-ray experiments, and H. Casalta for a critical reading of the manuscript.

[1] L. Néel, Ann. Geophys. **5**, 99 (1949).
[2] S. Morup, Hyperfine Interact. **60**, 959 (1990).
[3] F. Bodker, S. Morup, and S. Linderoth, Phys. Rev. Lett. **72**, 282 (1994).
[4] M. Ernst, J. Schelten, and W. Schmatz, Phys. Status Solidi A **7**, 469 (1971).
[5] S. Itoh, Y. Endoh, S. Taketomi, and S. Chikazumi, J. Magn. Magn. Mater. **103**, 126 (1992).
[6] R. Rosman, J. J. M. Janssen, and M. Th. Rekveldt, J. Appl. Phys. **67**, 3072 (1990).
[7] R. Childress, C. L. Chien, J. J. Rhyne, and R. W. Erwin, J. Magn. Magn. Mater. **104-107**, 1585 (1992).
[8] I. Mirebeau, C. Bellouard, M. Hennion, J. L. Dormann, C. Djega-Mariadassou, and M. Tessier, J. Magn. Magn. Mater. **104-107**, 1560 (1992).
[9] J. L. Dormann, C. Sella, P. Renaudin, and P. Gibart, Thin Solid Films **58**, 265 (1979).
[10] C. Djega-Mariadassou, J. L. Dormann, M. Nogues, G. Villers, and S. Sayouri, IEEE Trans. Magn. **26**, 1819 (1990).
[11] A. Guinier and G. Fournet, *Small Angle Scattering of X rays* (Wiley, New York/Chapman and Hall, London, 1955).
[12] N. W. Ashcroft and J. Lekner, Phys. Rev. **145**, 83 (1966).
[13] J. S. W. Lovesey, *Theory of Neutron Scattering from Condensed Matter* (Oxford Science, London, 1984).
[14] C. Bellouard, I. Mirebeau, and M. Hennion, J. Magn. Magn. Mater. **140-144**, 431 (1995).
[15] J. P. Bouchaud and P. G. Zerah, J. Appl. Phys. **70**, 6164 (1991).
[16] C. Bellouard, M. Hennion, and I. Mirebeau, J. Magn. Magn. Mater. **140-144**, 357 (1995).
[17] M. Hennion, C. Bellouard, and I. Mirebeau, Europhys. Lett. **25**, 43 (1994).
[18] J. L. Dormann, L. Bessais, and D. Fiorani, J. Phys. C **21**, 2015 (1988).
[19] M. Hennion, C. Bellouard, I. Mirebeau, J. L. Dormann, and R. Ober, J. Appl. Phys. **75**, 5900 (1994).